Climate windows for Polynesian voyaging to New Zealand and Easter Island

Ian D. Goodwin[a,1], Stuart A. Browning[a], and Atholl J. Anderson[b]

[a]Marine Climate Risk Group and Department of Environment and Geography, Macquarie University, Sydney, NSW 2109, Australia; and [b]Research School of Asia-Pacific, Australian National University, Canberra, ACT 2001, Australia

Edited by Patrick V. Kirch, University of California, Berkeley, CA, and approved August 13, 2014 (received for review May 14, 2014)

Debate about initial human migration across the immense area of East Polynesia has focused upon seafaring technology, both of navigation and canoe capabilities, while temporal variation in sailing conditions, notably through climate change, has received less attention. One model of Polynesian voyaging observes that as tradewind easterlies are currently dominant in the central Pacific, prehistoric colonization canoes voyaging eastward to and through central East Polynesia (CEP: Society, Tuamotu, Marquesas, Gambier, Southern Cook, and Austral Islands) and to Easter Island probably had a windward capacity. Similar arguments have been applied to voyaging from CEP to New Zealand against prevailing westerlies. An alternative view is that migration required reliable off-wind sailing routes. We investigate the marine climate and potential voyaging routes during the Medieval Climate Anomaly (MCA), A.D. 800–1300, when the initial colonization of CEP and New Zealand occurred. Paleoclimate data assimilation is used to reconstruct Pacific sea level pressure and wind field patterns at bidecadal resolution during the MCA. We argue here that changing wind field patterns associated with the MCA provided conditions in which voyaging to and from the most isolated East Polynesian islands, New Zealand, and Easter Island was readily possible by off-wind sailing. The intensification and poleward expansion of the Pacific subtropical anticyclone culminating in A.D. 1140–1260 opened an anomalous climate window for off-wind sailing routes to New Zealand from the Southern Austral Islands, the Southern Cook Islands, and Tonga/Fiji Islands.

proxy climate | Modoki La Nina

Archaeological, paleoenvironmental, and linguistic evidence of colonization in East Polynesia suggests that central East Polynesia (CEP) (Fig. 1) was colonized from Samoa about A.D. 1025–1120 and the marginal archipelagos, Hawaii, Easter Island, and New Zealand, about A.D. 1190–1290, with New Zealand reached from the Southern Cook or Austral Islands and Easter Island through the Gambier Islands (1, 2). On other analytical assumptions, the ages could be a century or so earlier (3). It is argued that long-distance voyaging later declined and had effectively ceased by A.D. 1500 (4, 5). One view is that colonization voyaging involved some capacity to sail to windward, assuming that modern climate patterns dominated the voyaging period (4, 6–8). This, together with the view that short-lived tradewind reversals associated with seasonal westerlies or El Niño events may have assisted voyaging, is reflected in the actual and simulated operation of experimental East Polynesian sailing canoes (4, 6–9). However, comparative analysis of the earliest historical observations and linguistic data suggests that, before contact with lateen-sail technology in West Polynesia, after about A.D. 1500, East Polynesian double canoes had no fixed mast and were restricted substantially to passages in the off-wind sector (10–12).

The advantage of off-wind passages, if they are available, is that broad-reaching (taking the wind on either quarter) or sailing downwind avoids the mechanical stresses of beating upwind and the necessity, by tacking, of having to sail up to four times the distance to reach the same objective (6, 9). Short eastward passages were possible in seasonal westerlies and long-distance passages off-wind could have occurred when westerly winds under very strong El Niño conditions created extensive subtropical tradewind reversals, but these were probably brief episodes and quite unpredictable (5, 7, 13–15). While the drivers of Polynesian migration are not known, any intentional or systematic sailing involved in colonization voyaging, whether by vessels with only a downwind capacity or those with greater capability, would have benefited from multidecadal-scale shifts to favorably fair winds. Such conditions occur for sailing into the extratropics when tropical and subpolar air masses, traveling as high-pressure systems, migrated poleward from their mean climate position in the subtropics (the location of highest subtropical pressure is along the Subtropical Ridge, STR), weakening the prevailing zonal westerlies in favor of meridional winds (16). Modern reenactments of Polynesian voyages (4, 6) show downwind sailing into the extratropical southwest Pacific is possible when northeast tradewinds replace seasonal westerlies in austral winter and spring.

Sea level pressure anomalies (SLPa) over the subtropical to extratropical Southern Hemisphere have been reconstructed recently for multidecadal time periods during the Medieval Climate Anomaly (MCA) (17). The MCA comprises two climate regimes, A.D. 800–1100 and A.D. 1100–1300, each with differently anomalous austral winter and spring seasonal climates compared with the modern climate.

The bidecadal to centennial climate shifts in the Pacific region during the MCA can be described in terms of the latitudinal extent of the tropics and the mean state of the Pacific Ocean region with respect to the persistence or frequency of either phase of the El Niño–Southern Oscillation (ENSO). Shifts in mean climate state result from a change in the timing and frequency of persistent seasonal summer–winter weather patterns,

Significance

South Pacific migration routes used in East Polynesian colonization (A.D. 800–1500) have been assumed to be commonly upwind, when based on an understanding of modern climate patterns. Instead, our novel paleowind field reconstructions at bidecadal resolution show that migration routes lay downwind from East Polynesia during known times of initial colonization of New Zealand and Easter Island. This finding is significant in showing that a windward seafaring capacity in Polynesian colonization voyaging was not essential, and that long-term temporal variation in sailing conditions due to the expansion of the tropics was important in shaping colonization histories. The paleoclimate reconstruction broadens colonization possibilities, and the method represents a new, globally applicable approach to understanding patterning in prehistoric maritime migration.

Author contributions: I.D.G. designed research; I.D.G. and S.A.B. performed research; I.D.G., S.A.B., and A.J.A. analyzed data; I.D.G., S.A.B., and A.J.A. wrote the paper; and I.D.G. and S.A.B. drafted figures.

The authors declare no conflict of interest.

This article is a PNAS Direct Submission.

[1]To whom correspondence should be addressed. Email: Ian.Goodwin@mq.edu.au.

This article contains supporting information online at www.pnas.org/lookup/suppl/doi:10.1073/pnas.1408918111/-/DCSupplemental.

www.pnas.org/cgi/doi/10.1073/pnas.1408918111

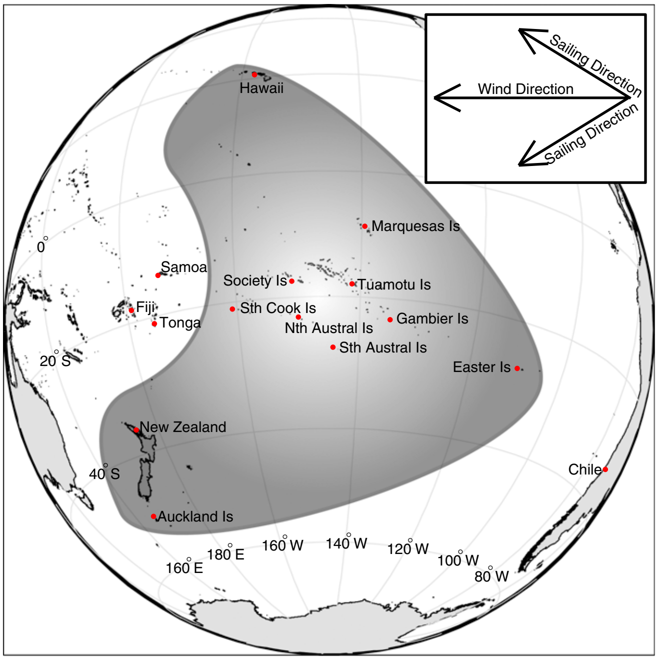

Fig. 1. Pacific Ocean region showing the greater portion of the Polynesian Colonization triangle across the Central Eastern Pacific (CEP), extratropical southwest Pacific, and subtropical North Pacific that was colonized post-A.D. 1000. The Samoa Islands and Tonga Islands were colonized in an earlier migration episode circa 3,000 y B.P. (*Inset*) The range of off-wind sailing directions assumed here for Polynesian sailing canoes: directly downwind plus up to ±30° to each side of that.

and storm frequency. For example, a shift to more El Niño-like (La Niña-like) climate involves a higher frequency of westerly (southeasterly) winds in the Southern Hemisphere tropics and, on a decadal scale, represents the occurrence of multiyear El Niño (La Niña) events, as seen in recent decades 1980–2000 (1950–1970). Similarly, a poleward expansion (equatorward contraction) of the tropics results in more (less) frequent, quasi-stationary anticyclones in the subtropics, and more (less) north–south (west–east) winds in the southwest Pacific.

During A.D. 800–900 and A.D. 1000–1100, the centennial mean climate pattern resembles a shift to the Central Pacific (Modoki) El Niño pattern, with southwesterly wind fields over New Zealand, and anomalous westerly wind fields (trade wind reversals) over the Central Pacific, combined with a poleward tropics (17). The Pacific region during the intervening A.D. 900–1000 period was dominated by the El Niño pattern and equatorward tropics, where the westerly wind field anomalies are located in the western to central Pacific. From A.D. 1000-1300, the Pacific tradewinds were strengthened generally by the poleward expansion of the tropics and the related, persistent subtropical anticyclones, firstly located over eastern and southern Australia and the Tasman Sea before A.D. 1100, then later over New Zealand and eastward post-A.D. 1140 (17). During A.D. 1140–1260, the Pacific was dominated by a shift in mean climate to the Central Pacific (Modoki) La Niña pattern, together with an intensification and poleward expansion of the subtropical anticyclone (17). The post-A.D. 1140 patterns impact the CEP via cool sea surface temperatures (SSTs) and drought in the tropical central Pacific, and bifurcation of tradewinds and surface currents in the vicinity of the Austral and Tuamotu Islands (18). Hence, the poleward expansion of the tropics during the MCA opened an anomalous climate window for off-wind sailing routes to the southwest Pacific extratropics, primarily New Zealand.

Our previous climate reconstructions (17) indicate that after A.D. 1300, no other multidecadal-scale climate windows occurred for reliable off-wind sailing between the subtropics and the southwest extratropics except for a brief period in the mid-1400s. The return to zonal midlatitude westerlies and subtropical easterly trades largely eliminated the climate windows for off-wind sailing on the routes at issue as a more persistent El Niño-like climate and equatorward subtropics dominated the South Pacific ~A.D. 1300 to ~A.D. 1600 (19–23).

These climate windows were investigated at bidecadal resolution in this study, using the paleoclimate proxy-data-assimilation approach (17) to reconstruct in additional detail the sea level pressure and surface wind field anomalies (with respect to the long-term mean climate for the A.D. 1300–2010 period). The reconstructions were determined for each running, 20-y window between A.D. 800 and A.D. 1600, spanning the austral winter (June, July, August) and spring (September, October, November) seasons (*Materials and Methods* and *SI Appendix*). The data assimilation approach preserves modeled intervariable relationships; therefore both sea level pressure and wind field reconstructions are dynamically consistent. To discuss potential canoe voyaging routes in more detail, we produced an envelope of surface wind directions at each grid point in the reconstruction to identify the off-wind sailing vector (directly downwind plus a margin of ±30° to allow for broad-reaching). We examined the significant surface wind anomalies for each 20-y window and plotted potential sailing routes from the central and southeast Pacific that would have resulted in landfalls in either New Zealand or Easter Island.

Several assumptions are made in the bidecadal climate reconstruction (see *Materials and Methods* and *SI Appendix*) that result in the following uncertainties, such as: proxy dating uncertainty, isolation of the proxy climate signal from nonclimatic noise, the limited spatial distribution of available proxy data, climate model limitations, and the assimilation algorithm. We have minimized dating uncertainties by resolving a bidecadal temporal resolution that is within estimated dating uncertainties for the included proxy data. Climate signal to noise uncertainties are minimized by evaluating proxy signal strength at each time step and including only proxies that display an unambiguous signal. The reconstructions are partly constrained by the geographic density of available proxy data for each window, in that the greater density allows for more redundancies in regional-scale reconstruction. The spatial distribution of proxy data is shown in *SI Appendix*, Fig. S1. The greater density of proxy data reduces any uncertainties in the bidecadal climate signal as a result of any inherent chronological data ambiguities or age range for each paleoclimate proxy. Hence, in this study, the greater density of paleoclimate data post-A.D. 1100 (*SI Appendix*, Fig. S2) affords greater certainty in the reconstruction of the regional synoptic climatology than before A.D. 1100.

Results and Discussion

The earliest MCA climate windows for off-wind sailing from the CEP to Easter Island occurred with persistent westerly wind anomalies during A.D. 800–820, A.D. 830–910, A.D. 1010–1030, A.D. 1040–1060, and A.D. 1080–1100 (*SI Appendix*, Fig. S5 *A* and *B*), with the latter dates coincident with initial CEP colonization (2). The wind fields from A.D. 830–850 and A.D. 860–890 show strong southeast to east sailing routes from Samoa to Easter Island, via the Gambier Islands or Austral Islands groups. Easter Island sailing routes originating in the Gambiers around A.D. 1250 and particularly from the Australs A.D. 1250–1280 were also afforded by westerly winds (*SI Appendix*, Fig. S5*C*). Both of these island groups are likely points of origin for passages to Easter Island, and both have colonization estimates (Rapa Island in the Southern Australs A.D. 1100–1200; Gambiers 1108–1275) contemporaneous with those for Easter Island (A.D. 1200–1253) (1, 2, 24). Nevertheless, voyaging at A.D. 800–900 cannot be discounted. It is interesting to note that the wind field reconstruction post-A.D. 1080 (Fig. 2*A*) seems to favor a migration origin in the Australs (latitude 25°S–27°S) over the commonly hypothesized route from the Gambiers (latitude 23°S). This supports a previous hypothesis that Polynesians voyaging eastward may have sailed in the ~28°S band that experiences a seasonal transition between southeast trades and westerlies in modern climate (9). The Australs to Easter Island route was also open: A.D. 1290–1440, A.D. 1500–1540, A.D. 1550–1570, and A.D. 1590–1610 (*SI Appendix*, Fig. S5*D*). These latter voyaging windows resulted from a contraction of the tropics and subtropics, and an equatorward shift in the westerlies, that occurred in association with a shift in mean climate state toward persistent El Niño conditions (19–23).

Return voyaging from Easter Island to CEP was possible when a climate shift restored easterly and northeasterly wind anomalies in the subtropical central Pacific at A.D. 1090–1120 and A.D. 1200–1250 (*SI Appendix*, Fig. S5 *B* and *C*). A strong anticyclonic wind field associated with easterly migration of the subtropical anticyclone to the east of New Zealand and a strengthened STR farther eastward provided reliable tradewinds and opened off-wind sailing routes for return voyaging from Easter Island to CEP. The wind fields in A.D. 1110–1130, A.D. 1200–1220, and A.D. 1230–1250 (*SI Appendix*, Fig. S5 *B* and *C*) show strengthened tradewinds between Easter Island and the Austral Islands, producing an off-wind route to the southern Australs. This east–west sailing route could have been readily navigated using latitudinal star path methods.

An alternative or additional hypothesis for settlement on Easter Island is voyaging by Amerindians from South America. Our reconstruction indicates off-wind sailing routes to Easter Island from Central and Northern Chile in A.D. 910–930, A.D. 930–950 (*SI Appendix*, Fig. S5*A*) and A.D. 1140–1170 (Fig. 2*B*), and A.D. 1220–1260 (Fig. 3 *A* and *B*). These follow the equatorward limb of the east Pacific Subtropical Anticyclone, in the Humboldt Current, angling northwest about 30°S, then westward toward Easter Island. Potential return routes to Chile were open A.D. 1260–1290, closing with strengthened southward flow around A.D. 1300 (Fig. 3*C* and *SI Appendix*, Fig. S5 *C* and *D*).

New Zealand sailing routes were possible as early as A.D. 910–970 (*SI Appendix*, Fig. S5*A*) and from A.D. 1140–1260 (Figs. 2*B* and 3*B*), when intensification of the subtropical anticyclone opened an anomalous climate window for off-wind sailing routes to the southwest Pacific extratropics. This climate pattern produced three potential routes to the New Zealand region: from the Southern Australs, the Southern Cooks, and Tonga/Fiji. Eventual New Zealand landfall on routes from the Southern Australs and the Southern Cooks was assisted by the Coriolis Effect in the Southern Hemisphere, which deflects the surface ocean current to the left (southwestward) of the subtropical surface wind field.

In A.D. 940–970 and between A.D. 1170–1230, potential sailing routes from the subtropical Pacific to New Zealand originated in Tonga and Fiji, and possibly even Vanuatu or New Caledonia. During A.D. 1170–1210 (A.D. 1170–1190 shown in Fig. 2*C*), off-wind sailing routes from Tonga take a southerly track before encountering northeasterly winds, around 35°S, that focus possible landfalls along the east coast of the South Island and southward to the subantarctic Auckland Islands. Early settlement in the latter group [A.D. 1190–1258, (2, 25)] might have profited from the existence of northerly or northeasterly winds,

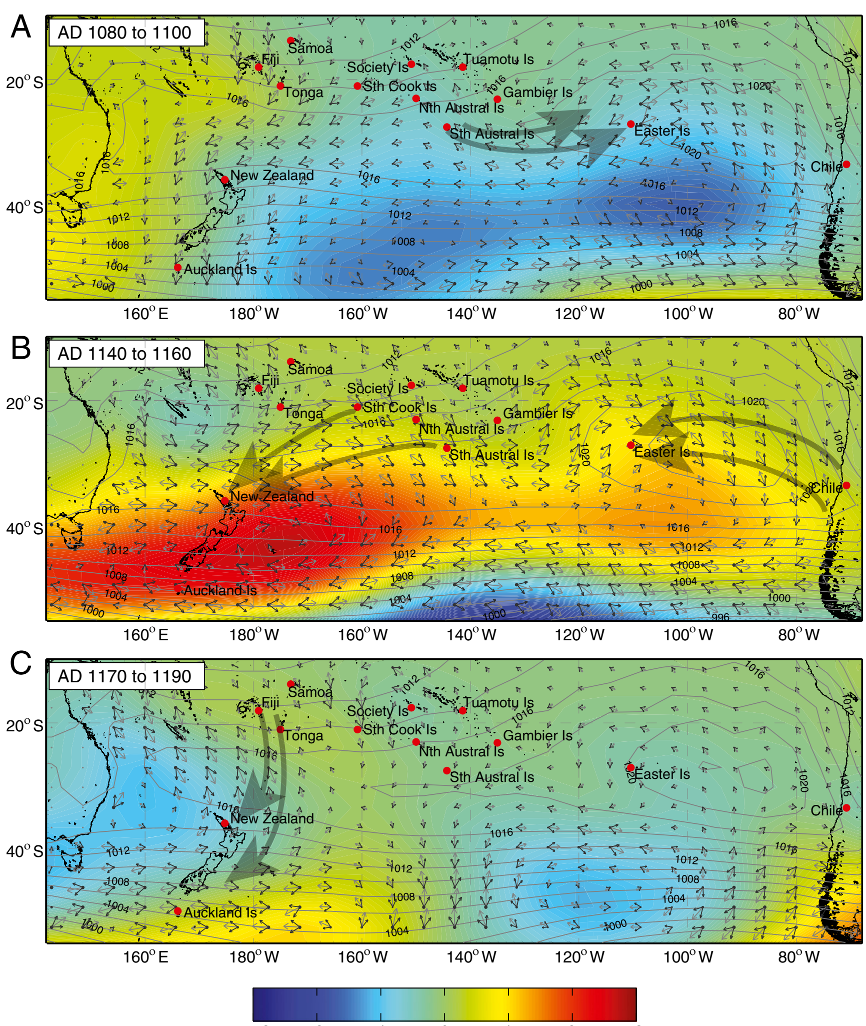

Fig. 2. Reconstructed bidecadal mean sea level pressure (black lines), sea level pressure anomalies (color, hectopascals), and the associated wind field anomaly vectors (gray) for the periods (*A*) A.D. 1080–1100, (*B*) A.D. 1140–1160, and (*C*) A.D. 1170–1190. Also shown, for each wind direction vector, is the ±30° limit of off-wind sailing vectors (solid black) for Polynesian canoe voyaging (after Fig. 1). The length of the wind anomaly and associated off-wind sailing vectors depict the relative difference in wind speed across the Pacific and are proportional to the reconstructed atmospheric pressure gradients. The potential downwind voyaging routes for each climate window are denoted by the large gray arrows.

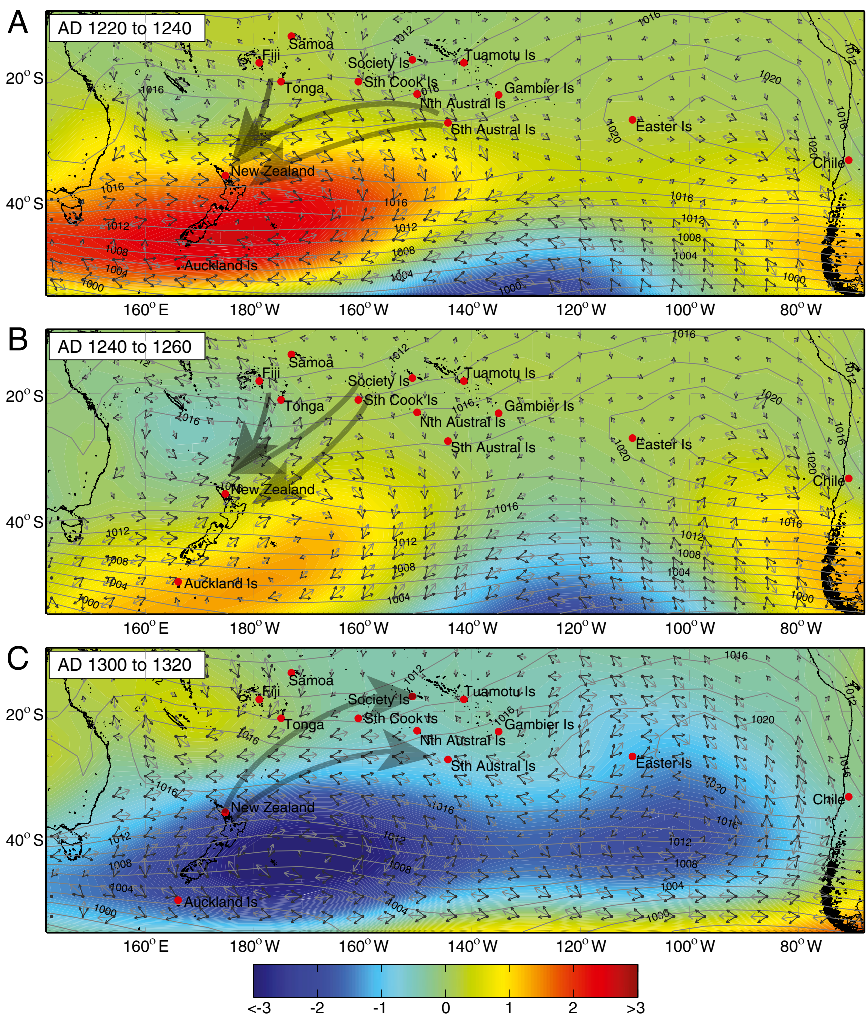

Fig. 3. Reconstructed bidecadal mean sea level pressure (black lines), sea level pressure anomalies (color, hectopascals), and the associated wind field anomaly vectors (gray), together with a ±30° off-wind sailing vectors for the periods (*A*) A.D. 1220–1240, (*B*) A.D. 1240–1260, and (*C*) A.D. 1300–1320. The potential downwind voyaging routes for each climate window are denoted by the large gray arrows.

which transport warm subtropical air masses to the subantarctic. The STR was located around 47°S at A.D. 1170–1210, its most southerly position during the MCA (17). This anomaly deteriorated after A.D. 1240 and disappeared after A.D. 1270 when austral winter–spring westerlies were restored over the Auckland Islands.

The earliest climate window for voyaging to New Zealand from the southern Australs is in A.D. 910–930 until A.D. 940–960, which predates archaeological estimates of Austral Islands colonization. This downwind route between the Southern Australs and New Zealand was also open in A.D. 1140–1170 (A.D. 1140–1160 shown in Fig. 2*B*), and A.D. 1200–1240 (A.D. 1220–1240 shown in Fig. 3*A*); these periods span modern archaeological estimates of colonization age (2, 3, 13). Canoes that sailed west in the 27°S to 30°S latitudinal band could have become caught in the strong east-northeasterlies produced by the intensified subtropical anticyclone over the southwest Pacific.

A downwind route existed between the Southern Cook Islands and New Zealand at A.D. 940–960 (*SI Appendix*, Fig. S5*A*) and from A.D. 1140–1160, A.D. 1210–1230, and particularly A.D. 1240–1260 (Figs. 2*B* and 3*B*), with persistent easterly tradewinds over the Southern Cooks, becoming northeasterly near the dateline. Most sailing routes from possible southern Cook or Austral origins focus landfall possibilities on the northeast coast of the North Island of New Zealand, consistent with Maori traditions about colonization canoe landfalls.

Return voyaging from New Zealand to CEP required southwesterlies to the Southern Cooks and westerlies in the ∼30°S latitudes to the Southern Australs. These conditions occurred in A.D. 960–990 but became prevalent from the mid-1200s. Return voyaging to the Southern Cooks is constrained to A.D. 1280–1300, while return voyaging to the Southern Australs has a longer window from A.D. 1250–1270 and post-1300 (Fig. 3*C*), until the early 1600s. These periods were interspersed with a potential window, A.D. 1270–1290 for voyaging back to New Zealand from the Australs. Hence, opportunities for three-way voyaging on a bidecadal scale occurred briefly due to an equatorward shift in the STR and the seasonal persistence of traveling anticyclones.

Our wind field reconstructions indicate that no other bidecadal-scale climate windows for reliable off-wind sailing between the subtropics and the southwest Pacific extratropics existed post-A.D. 1260 (except for a period, A.D. 1440–1460, *SI Appendix*, Fig. S5*D*), as El Niño-like conditions prevailed up to ∼A.D. 1600 (19–23), and more zonal midlatitude westerlies and subtropical easterly trades were restored (*SI Appendix*, Fig. S5*D*). This does not preclude individual years from presenting favorable seasonal-scale wind fields for downwind sailing between the subtropical Pacific and New Zealand, but it does emphasize that these conditions would not be normal, or reliable across generations.

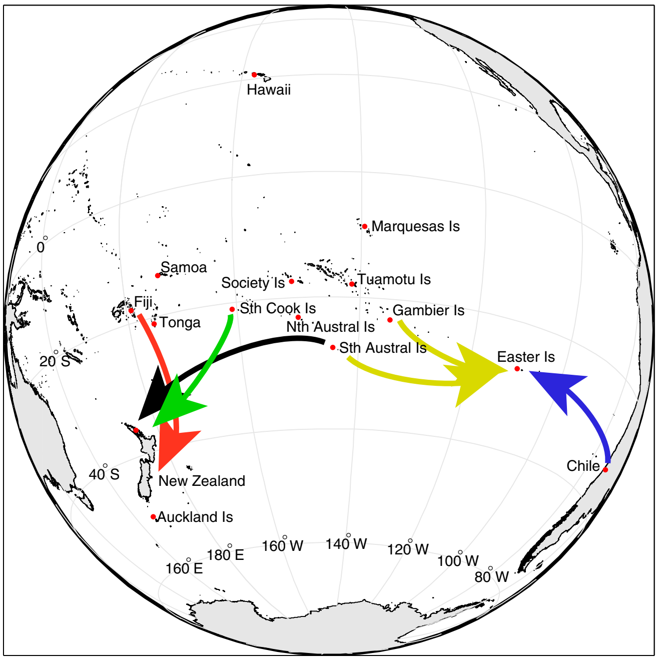

Fig. 4. Potential Polynesian voyaging routes to the CEP and extratropical southwest Pacifc post-A.D. 800 are shown. The red route was open between A.D. 940–970 and between A.D. 1170–1210. The green route was open A.D. 940–960, A.D. 1140–1160, A.D. 1210–1230, and A.D. 1240–1260. The black route was open A.D. 910–960, A.D. 1140–1170, and A.D. 1200–1240. The yellow routes were open from A.D. 800–910, A.D. 1010–1030, A.D. 1040–1060, A.D. 1080–1100, and A.D. 1250–1280. The more southern route from the Austral islands was open from A.D. 1290 to A.D. 1440, A.D. 1500–1540, A.D. 1550–1570, and A.D. 1590–1610. The blue route was open from A.D. 910–950, 1140–1170, and A.D. 1230–1250. Return voyaging along the green and black routes was open in A.D. 960–990, and mainly open from A.D. 1260 to A.D. 1550.

Hence, our wind field reconstructions are consistent with the archaeological evidence that long-distance voyaging to New Zealand either ceased or was rare after A.D. 1300.

In summary, there were multidecadal climate windows for off-wind voyaging during the MCA, (Fig. 4) from: (*i*) CEP to Easter Island between A.D. 800 and A.D. 900, A.D. 1000 and A.D. 1100, and during A.D. 1250–1280; (*ii*) the eastern margins of far East Polynesia (including Easter Island), in a northwestward direction, particularly A.D. 1140–1160, and A.D. 1180–1250; and (*iii*) CEP to New Zealand in A.D. 910–960 and A.D. 1140–1260. The A.D. 1100–1300 windows are all consistent with current archaeological and related evidence. Additional windows between Tonga/Fiji and New Zealand during A.D. 940–970 and A.D. 1170–1230 provide potential for investigating cultural connections otherwise generally discounted. Our data also show that return voyaging was periodically possible by off-wind sailing in each direction, and we document a wider range of off-wind voyaging opportunities than those currently envisaged, including between the Australs and Easter Island, between Fiji or Tonga and New Zealand, and between Easter Island and extratropical Chile.

Our reconstructed sailing conditions during the period of East Polynesian colonization would have enabled all of the known colonizing routes, and others, to have been negotiated at times proposed archaeologically by canoes lacking an upwind capability. We do not assert that this ability was absent, although it may have been (10–12). Our point is that the climatic evidence suggests that an upwind capability was not necessary for exploration and colonization of the remote East Polynesian islands during the periods attested archaeologically. In addition, an absence of effective upwind capability might have been significant in the decline of long-distance voyaging in East Polynesia once the sailing windows discussed here had closed. Furthermore, societal response to drought in CEP associated with the Modoki La Niña pattern may have been influential in decisions to migrate, as disputes about land and garden produce figure prominently in tradition as the particular cause of migrations from CEP to the outlying archipelagos (26). Our results suggest that current models of Polynesian maritime technology during the MCA (27, 28) and simulated and experimental voyaging need to be reconsidered. We conclude that climate change provided ample opportunity for Polynesian migration by off-wind sailing during the Late Holocene.

Materials and Methods

Methods. Mean sea level pressure (SLP) and wind fields for the South Pacific basin have been reconstructed at 20-y resolution from A.D. 800–1600 using an established and previously described (17) paleoclimate data assimilation approach. Our approach to data assimilation builds on other previous methods (23, 29) by using the combined signal from a multivariate proxy data network to select climate state analogs from an existing ensemble. This section describes the standardization of proxy and model data, analog selection, and calculation of reconstructed SLP and wind fields. The *SI Appendix* contains: the proxy network (*SI Appendix*, Fig. S1 and Table S1), the results of a pseudoproxy methodological evaluation (*SI Appendix*, Fig. S3), the proxy signal used to reconstruct each time period in Figs. 2 and 3 and *SI Appendix*, Fig. S4, and the bidecadal time period reconstructions referred to in *Results and Discussion* from A.D. 800–1600 (*SI Appendix*, Fig. S5 *A–D*).

Proxy Records. The multivariate proxy dataset includes individual proxy records, reconstructions, and published regional multiproxy reconstructions (*SI Appendix*, Fig. S1 and Table S1). Before assimilation, all annually resolved proxy data were resampled to decadal values, decadally resolved data were used without resampling, and discrete proxy climate data were binned to decadal values. To facilitate the intercomparison of proxy data representing different variables, all decadal data were normalized relative to the A.D. 1300–2000 long-term mean. The mean climate signal for each proxy was calculated for each discrete 20-y time period. In acknowledgment of the high signal-to-noise ratio associated with proxy data, each 20-y period was reconstructed using only proxies displaying an unambiguous climatic signal (*SI Appendix*, Fig. S4), defined as the 20-y mean exceeding ± 0.5 SD. The normalized values for each retained proxy were combined into a vector (**P**) for each 20-y time period (*SI Appendix*, Fig. S4).

Model and Simulation Setup. The model simulation used in this study is a 10,000-y Holocene control simulation from the Commonwealth Scientific and Industrial Research Organization (CSIRO) Mk3L climate system model version 1.2. The Mk3L model is a fully coupled reduced-resolution global atmosphere–land–sea ice–ocean general circulation model designed specifically for millennial-scale climate simulations (30). The atmospheric component of Mk3L is a computationally efficient version of the atmospheric component of the Mk3 model used in World Climate Research Programme Coupled Model Intercomparison Project Phase 3 (WCRP-CMIP3) and the Intergovernmental Panel on Climate Change Fourth Assessment Report (30, 31). The model incorporates a 5.6×3.2 degree atmosphere with 18 vertical levels and a 2.8×1.6 degree ocean with 21 vertical levels; a more detailed description can be found in ref. 30. The model simulates a modern-day climate reasonably well, including a realistic ENSO, albeit with some biases outlined in ref. 32. The Mk3L also produces a realistic simulation of the amplitude and spatial characteristics of the high-latitude modes, the Southern Annular Mode, and Pacific South American Modes 1 and 2 (17). The 10,000-y simulation used in this study is an unforced control simulation of Holocene climate with constant boundary conditions: CO_2 set to 280 ppm, solar irradiance set to 1365 W m^{-2}, and A.D. 1950 orbital parameters. An additional model simulation, an A.D. 800–2000 Mk3L transient simulation forced with reconstructed solar (33), volcanic (34) and CO_2 (35), is used as the target climate for a pseudoproxy evaluation (*SI Appendix*, Fig. S3). To assimilate model and proxy data, both must be in a standardized format. The model data are therefore represented by an array of normalized annual mean timeseries (*S*) derived from the same variables and locations as the proxy records in **P**. To account for seasonality, annual means were calculated from the seasons of proxy sensitivity.

Paleoclimate Data Assimilation. The paleoclimate data assimilation approach uses the combined signals from multiple proxy records to select climate state analogs from the model simulation (23, 29). Each model time step represents a dynamically consistent multivariate realization of the climate system that is a potential analog for a paleoclimate state. In this sense, each model time step can be considered to be an individual ensemble member, giving an effective ensemble size of 10,000. Individual ensemble members analogous to the proxy inferred climate states for each 20-y period were identified by calculating the Euclidean distance between the normalized proxy data (**P**) and the normalized model data ($S_{1\text{-}n}$) as shown in Eq. **1**:

$$D_n = \sum |\mathbf{P}_i - S_{ni}|. \qquad [1]$$

P is a vector (width = i) of normalized proxy values that succinctly describes the climate state for a given multidecadal time period. S is an array of timeseries (width = i and length = n) derived from the modeled climate at the equivalent geographic locations and climate variables as the elements of **P**. Each column of $S_{1\text{-}i}$ corresponds to each element of $\mathbf{P}_{1\text{-}i}$, and each row of $S_{1\text{-}n}$ represents one model ensemble member (one modeled year). D_n is the Euclidean distance between **P** and each ensemble member (n). Values of $D_n = 0$ indicate a perfect analog, while high values indicate dissimilarity. The best matching analog (BMA) ensemble members are the minima of $D_{1\text{-}n}$: The mean of the 50 BMA is used to define the climate state for the time period of interest. Any modeled variable can be resolved by compositing the 50 BMA ensemble mean; however, only modeled variables with a mechanistic relationship to the proxy dataset should be interpreted with confidence. The reconstructions presented here show the SLP and SLPa fields, with wind fields superimposed. Wind strength and directions were calculated from the ensemble means of the modeled U (east–west) and V (north–south) components at the 1,000-hPa level. Anomalies are calculated relative to the full 10,000-y simulation and therefore represent deviations from the modeled Holocene climate and are not directly representative of deviations from the climate of the Common Era. Spatial field reconstructions for time periods referred to in *Results and Discussion* are shown in *SI Appendix*, Fig. S5 *A–D*.

Evaluation. Methodological evaluation using pseudoproxy data show that the approach should accurately reconstruct SLP fields for most of the South Pacific Basin and Southern Ocean (see *SI Appendix*, Fig. S4). In the pseudoproxy experiment, a model simulation of the real climate is "reconstructed" using a synthetic proxy network; because the climate state to be reconstructed is already known, the skill of the reconstruction approach can be tested (after refs. 36 and 37). The known climate is an A.D. 800–2000 Mk3L simulation forced with reconstructed solar (33), volcanic (34), and CO_2 (35) conditions. Pseudoproxies were derived from the model simulation using the same variables and locations as the proxy network listed in *SI Appendix*, Table S1. A signal-to-noise ratio of 0.33 was added to each pseudoproxy to simulate real-world uncertainty (after ref. 38). The 1,200-y model simulation was then reconstructed at 20-y resolution using the multivariate data assimilation approach to select climate state analogs from the unforced 10,000-y simulation (see *Methods*) based only on the climate signals from the pseudoproxy network. *SI Appendix*, Fig. S3 shows grid point correlations between modeled and reconstructed SLP over 1,200 model years at 20-y resolution; it provides an indication of the skill of the reconstruction approach given the current proxy network (*SI Appendix*, Fig. S1 and Table S1). Positive correlations show increased reconstruction skill, while lower values indicate reduced skill. The actual SLP and wind field reconstruction, based on real proxy data, should be interpreted with the highest confidence in the regions indicated by significant positive correlations. The reconstruction attains higher levels of significance for periods of higher available proxy data geographic density.

ACKNOWLEDGMENTS. We thank two anonymous reviewers for their constructive comments. The research was partially funded by a Macquarie University External Collaborative Grant with the New South Wales Office for Environment and Heritage, and the New South Wales Environmental Trust (to I.D.G.). S.A.B. received a postgraduate Macquarie University Research Scholarship (MQRES). The climate reconstruction research forms a contribution to the Australian Eastern Seaboard Climate Change Initiative.

1. Kirch PV, Conte E, Sharp W, Nickelsen C (2010) The Onemea site (Taravai Island, Mangareva) and the human occupation of southeast Polynesia. *Archaeol Oceania* 45(2): 66–79.
2. Wilmshurst JM, Hunt TL, Lipo CP, Anderson AJ (2011) High-precision radiocarbon dating shows recent and rapid initial human colonization of East Polynesia. *Proc Natl Acad Sci USA* 108(5):1815–1820.
3. Mulrooney MA, Bickler SH, Allen MS, Ladefoged TN (2011) High-precision dating of colonization and settlement in East Polynesia. *Proc Natl Acad Sci USA* 108(23): E192–E194, and author reply (2011) 108(23):E195.
4. Irwin GJ (2006) Voyaging and settlement. *Vaka Moana: Voyages of the Ancestors—The Discovery and Settlement of the Pacific*, ed Howe KR (Bateman, Auckland, New Zealand), pp 56–91.
5. Irwin GJ (1992) *The Prehistoric Exploration and Colonisation of the Pacific* (Cambridge Univ Press, Cambridge, UK).
6. Finney BR (2006) Ocean sailing canoes. *Vaka Moana: Voyages of the Ancestors—The Discovery and Settlement of the Pacific*, ed Howe KR (Bateman, Auckland, New Zealand), pp 100–153.
7. Di Piazza A, Di Piazza P, Pearthree E (2007) Sailing virtual canoes across Oceania: Revisiting island accessibility. *J Archaeol Sci* 34(8):1219–1225.
8. Montenegro A, Callaghan R, Fitzpatrick S (2014) From west to east: Environmental influences on the rate and pathways of Polynesian colonization. *Holocene* 24(2): 242–256.
9. Finney BR (1985) Anomalous westerlies, El Niño and the colonisation of Polynesia. *Am Anthropol* 87(1):9–26.
10. Anderson AJ (2000) Slow boats from China: Issues in the prehistory of Indo-Pacific seafaring. *East of Wallace's Line*, eds O'Connor S, Veth P (Balkema, Rotterdam), pp 13–50.
11. Anderson AJ (2008) Forum: Traditionalism, interaction and long-distance seafaring in Polynesia. *J Island Coastal Archaeol* 3(2):240–270.
12. Anderson AJ (2014) Seafaring in remote Oceania: Traditionalism and beyond in maritime technology and migration. *Oxford Handbook of Oceanic Archaeology*, eds Hunt TL, Cochrane E (Oxford Univ Press, Oxford).
13. Anderson AJ (1991) The chronology of colonization in New Zealand. *Antiquity* 65(249):767–795.
14. Caviedes C (2001) *El Niño in History* (Univ of Florida Press, Gainesville, FL).
15. Anderson AJ, Chappell J, Gagan M, Grove R (2006) Prehistoric maritime migration in the Pacific Islands: An hypothesis of ENSO forcing. *Holocene* 16(1):1–6.
16. Bridgman HA (1983) Could climate change have had an influence on the Polynesian migrations? *Palaeogeogr Palaeoclimatol Palaeoecol* 41(3):193–206.
17. Goodwin ID, et al. (2014) A reconstruction of extratropical Indo-Pacific sea-level pressure patterns during the Medieval Climate Anomaly. *Clim Dyn* 43:1197–1219.
18. Shinoda T, Hurlburt HE, Metzger EJ (2011) Anomalous tropical ocean circulation associated with La Niña Modoki. *J Geophys Res* 116(C12001), 10.1029/2011JC007304.
19. Lorrey AM, et al. (2013) The Little Ice Age climate of New Zealand reconstructed from Southern Alps cirque glaciers: A synoptic type approach. *Clim Dyn* 42:3039–3060.
20. Mann M, et al. (2009) Global signatures and dynamical origins of the Little Ice Age and Medieval Climate Anomaly. *Science* 326(5957):1256–1260.
21. Emile-Geay J, Cobb K, Mann M, Wittenberg A (2012) Estimating central equatorial Pacific SST variability over the past millennium. Part 2: Reconstructions and implications. *J Clim* 26(7):2329–2352.
22. Fowler AM, et al. (2012) Multi-centennial ENSO insights from New Zealand forest giants. *Nat Clim Change* 2:172–176.
23. Graham NE, et al. (2007) Tropical Pacific—Mid-latitude teleconnections in medieval times. *Clim Change* 83(1-2):241–285.
24. Hunt TL, Lipo CP (2006) Late colonization of Easter Island. *Science* 311(5767): 1603–1606.
25. Anderson AJ (2005) Subpolar settlement in South Polynesia. *Antiquity* 79(306): 791–800.
26. Grey G (1885) *Polynesian Mythology and Ancient Traditional History of the New Zealand Race* (Brett, Auckland, New Zealand).
27. Howe KR, ed (2006) *Vaka Moana: Voyages of the Ancestors—The Discovery and Settlement of the Pacific* (Bateman, Auckland).
28. Pearce CEM, Pearce FM (2010) *Oceanic Migration: Paths, Sequence, Timing and Range of Prehistoric Migration in the Pacific and Indian Oceans* (Springer, Heidelberg).
29. Goosse H, Renssen H, Timmermann A, Bradley RS, Mann ME (2006) Using paleoclimate proxy-data to select optimal realisations in an ensemble of simulations of the climate of the past millennium. *Clim Dyn* 27(2-3):165–184.
30. Phipps SJ, et al. (2011) The CSIRO Mk3L climate system model version 1.0 – Part 1: Description and evaluation. *Geosci. Model Dev.* 4(2):483–509.
31. Meehl GA, et al. (2007) THE WCRP CMIP3 multimodel dataset: A new era in climate change research. *Bull Am Meteorol Soc* 88(9):1383–1394.
32. Phipps SJ, et al. (2012) The CSIRO Mk3L climate system model version 1.0 – Part 2: Response to external forcings. *Geosci Model Dev* 5(3):649–682.
33. Steinhilber F, Beer J, Fröhlich C (2009) Total solar irradiance during the Holocene. *Geophys Res Lett* 36(19):L19704.
34. Gao C, Robock A, Ammann C (2008) Volcanic forcing of climate over the past 1500 years: An improved ice core-based index for climate models. *J Geophys Res* 113(D23): D23111.
35. MacFarling Meure C, et al. (2006) Law Dome CO_2, CH_4 and N_2O ice core records extended to 2000 years BP. *Geophys Res Lett* 33(14):L14810.
36. Jones PD, et al. (2009) High-resolution palaeoclimatology of the last millennium: A review of current status and future prospects. *Holocene* 19(1):3–49.
37. Mann M, Rutherford S, Wahl E, Ammann CM (2007) Robustness of proxy-based climate field reconstruction methods. *J Geophys Res* 112(D12):D12109.
38. Bhend J, Franke J, Folini D, Wild M, Brönnimann S (2012) An ensemble-based approach to climate reconstructions. *Clim Past* 8(4):963–976.

ANTHROPOLOGY

ENVIRONMENTAL SCIENCES

SI Appendix

Climate Windows for Polynesian Voyaging to New Zealand and Easter Island

Authors: Ian D. Goodwin[1]*, Stuart A. Browning[1], Atholl J. Anderson[2]

Affiliations: [1]Marine Climate Risk Group and Department of Environment and Geography, Macquarie University, 2109, New South Wales, Australia
[2]Research School of Asia-Pacific, Australian National University, Canberra, ACT 2001, Australia

Supplementary Information:
Figures S1-S5
Table S1
References for SI Appendix

Supporting figures

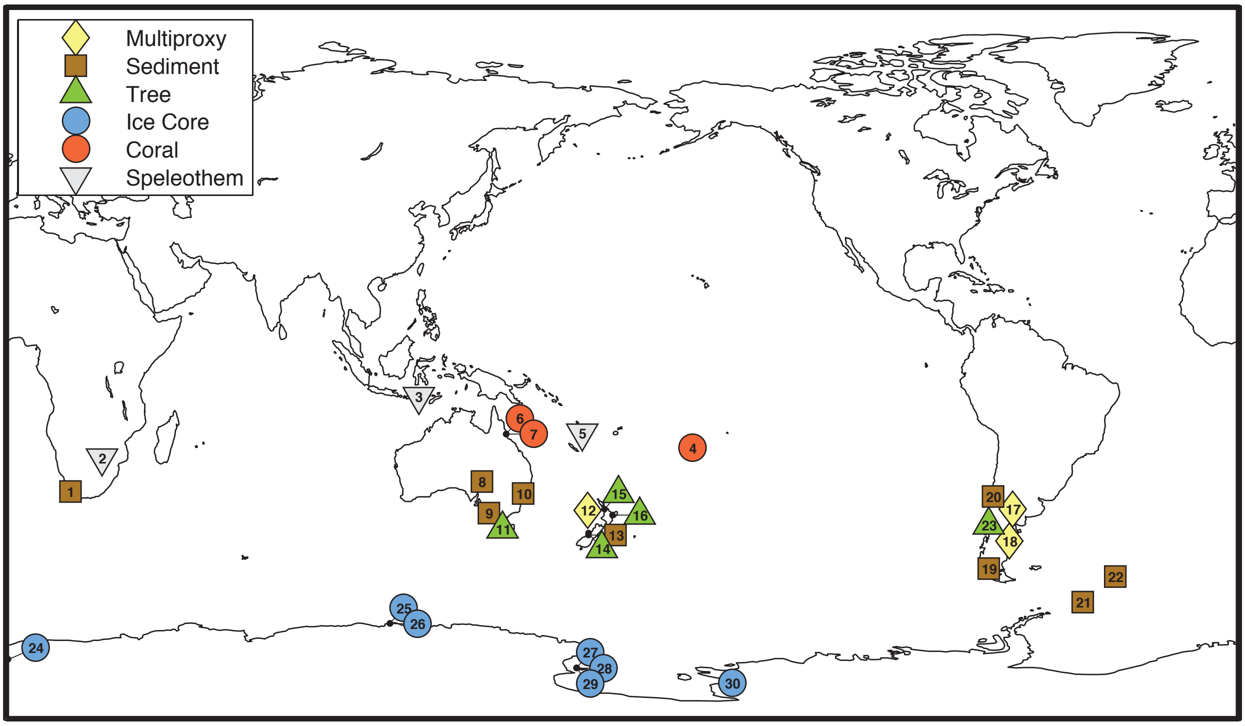

Figure S1: Map showing the locations and types of proxy data used in the reconstructions. Numbers correspond to individual records listed in SI Appendix, Table S1.

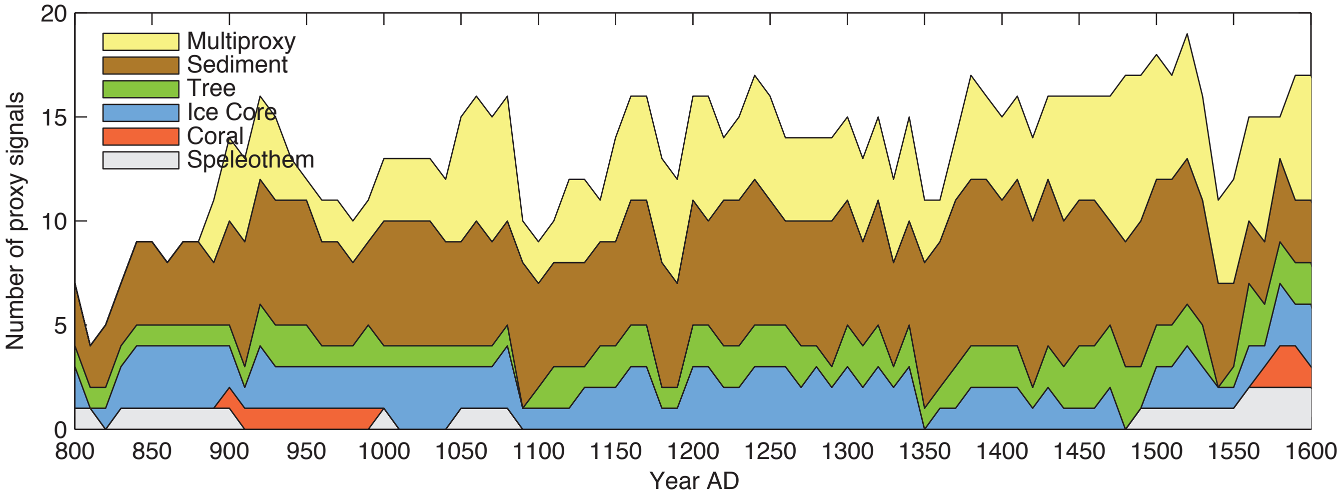

Figure S2: Illustration of the number of individual proxies used during each bi-decadal time period. Only proxies displaying an unambiguous climatic signal, defined as a 20-year normalised anomaly exceeding +/- 0.5 standard deviations (relative to the AD 1300-2000 long term mean) were included in the reconstruction for each bi-decadal period

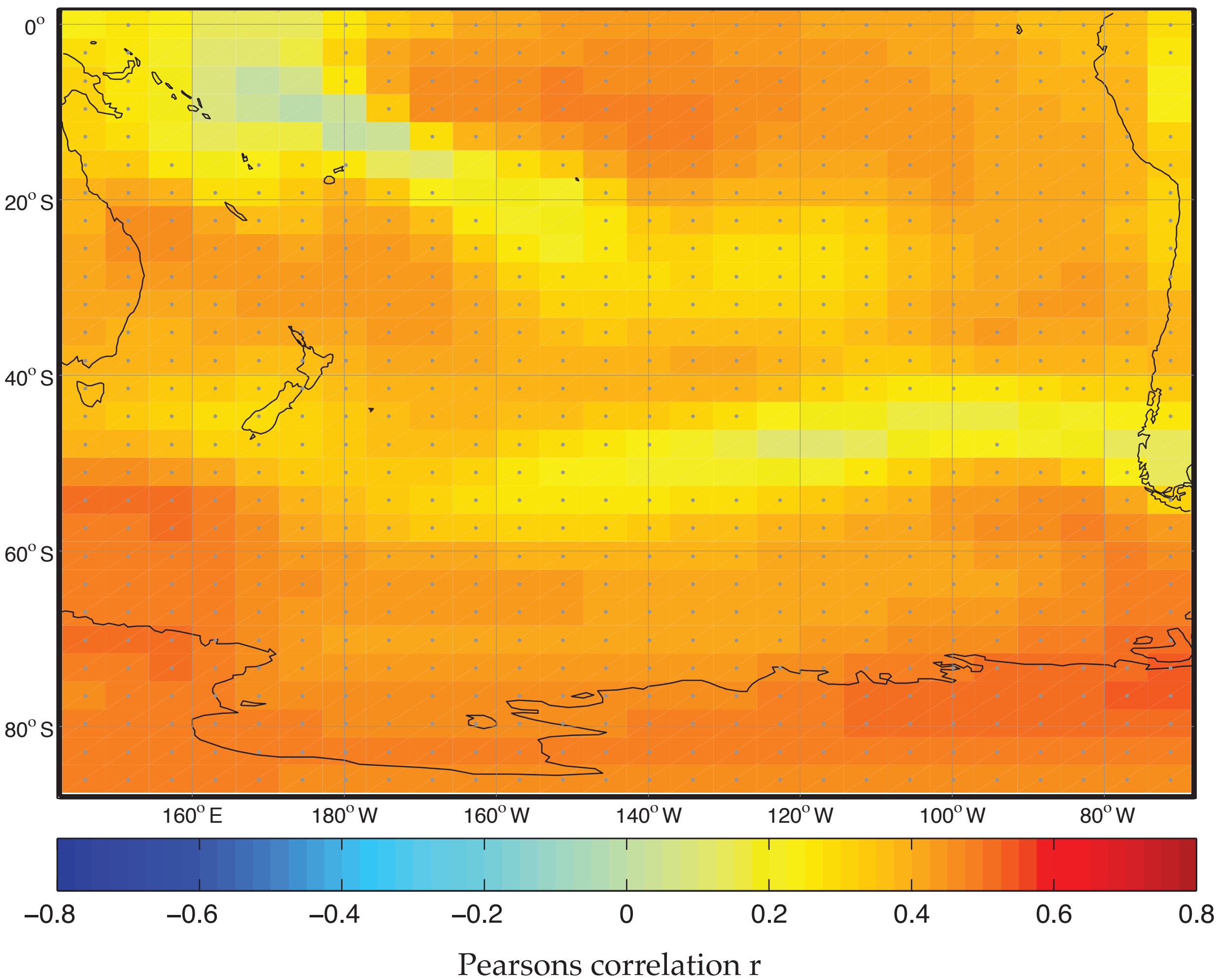

Figure S3: Evaluation of reconstruction skill using a pseudo proxy experiment. This figure shows grid point correlations between modelled and reconstructed sea level pressure (SLP) over 1200 model years at 20-year resolution. Stippling indicates correlations significant at the 99% level; positive significant correlations show increased reconstruction skill while lower values indicate reduced skill.

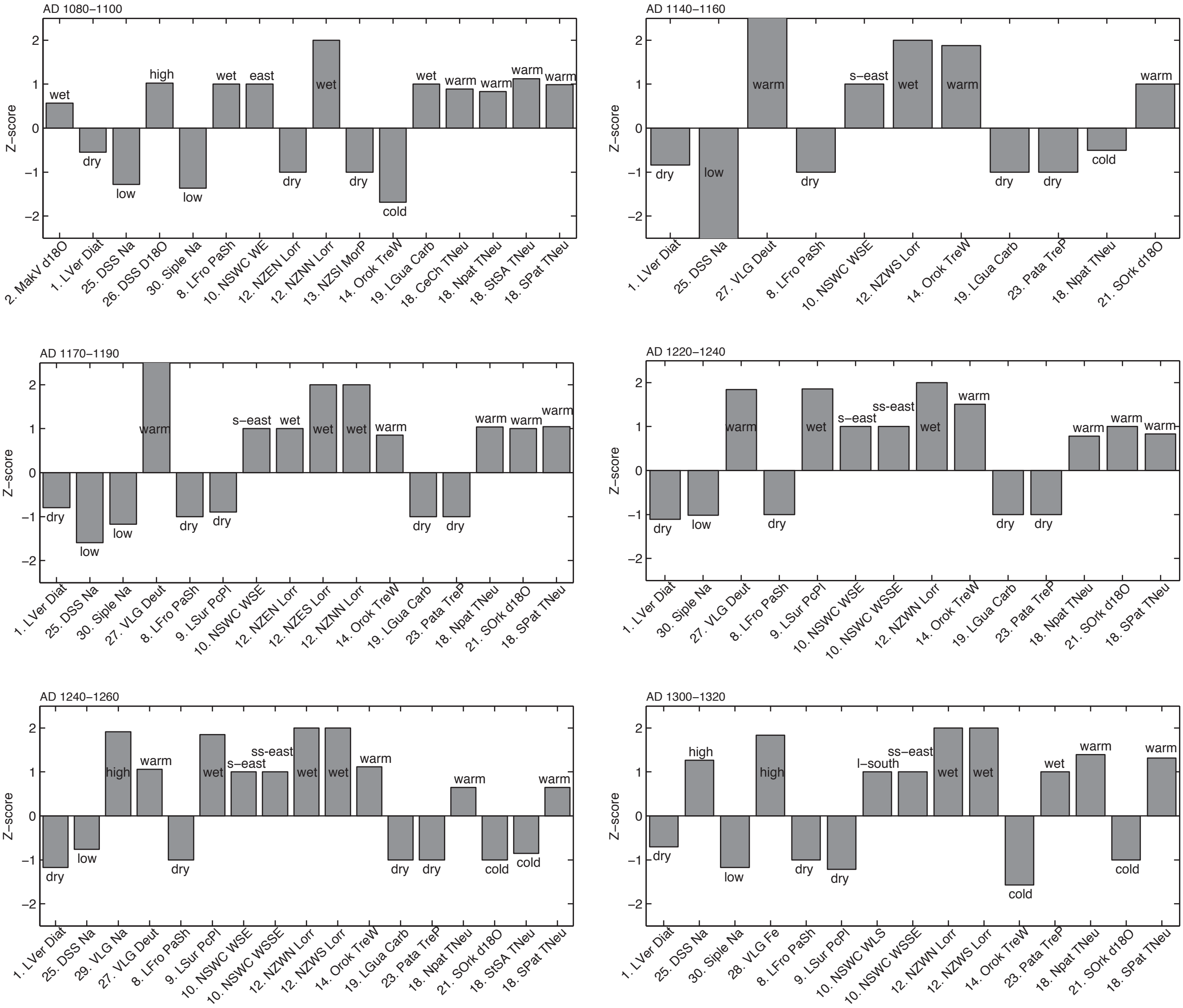

Figure S4: Proxy vectors (P) showing included proxies and climate signals for each of the six bi-decadal time periods shown in Fig. 2 and Fig. 3 (main document). The climate signal is defined as the normalised 20-year mean and corresponding ordinal classification. Proxy names are necessarily abbreviated—numbers correspond to individual proxy records listed in SI Appendix, Table S1 and mapped in SI Appendix, Fig. S1.

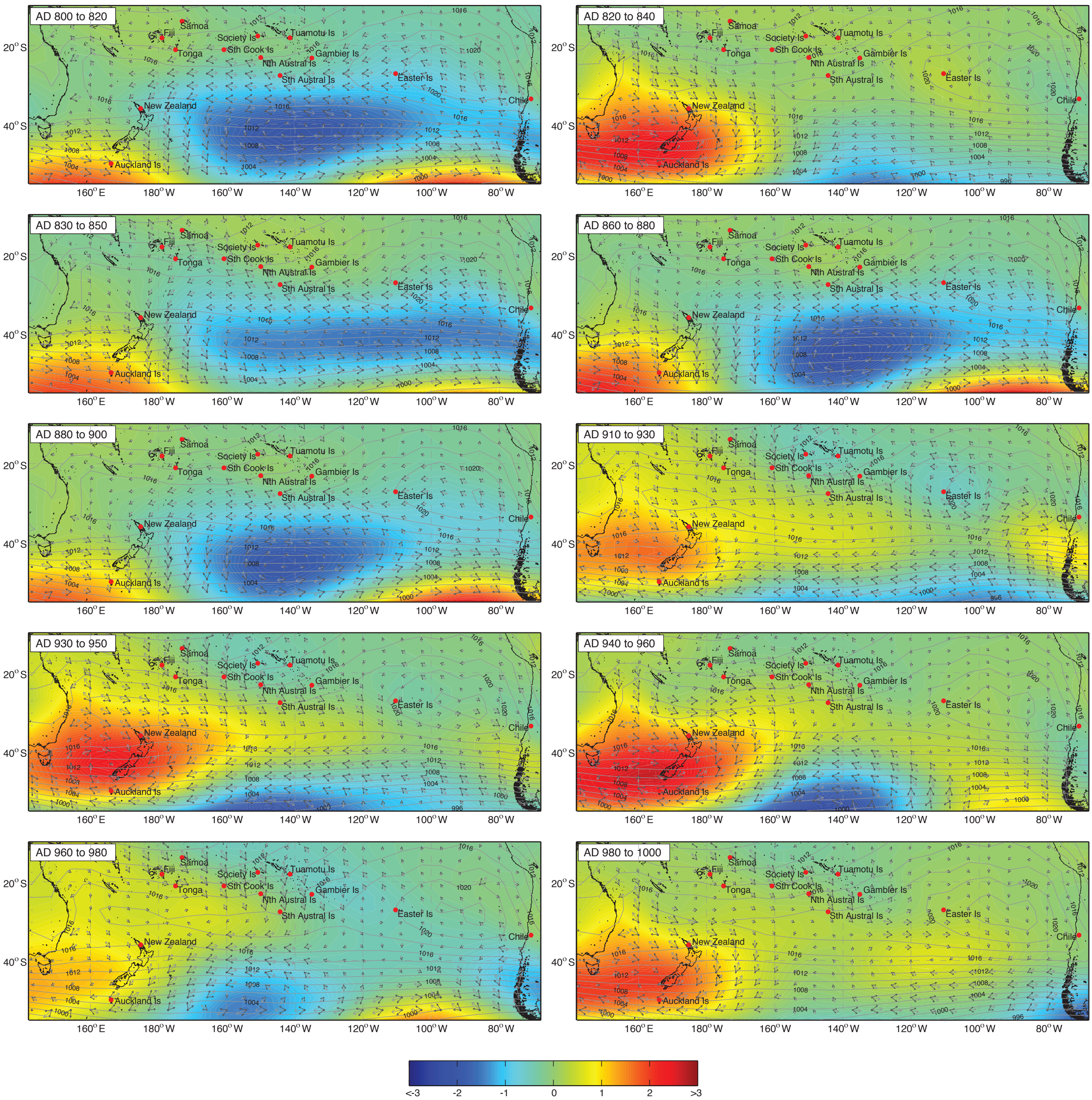

Figure S5a: Bi-decadal time period reconstructions. Each figure panel shows the reconstructed bi-decadal mean sea-level pressure (black lines), sea-level pressure anomalies (colour, hPa), and the associated wind field anomaly vectors (grey) for selected periods between AD 800 and 1000, as referred to in the main text. Also shown for each wind direction vector, is the ± 30° limit of off-wind sailing vectors (solid black) for Polynesian canoe voyaging (after Fig. 1, main document). The length of the wind anomaly and associated off-wind sailing vectors depicts the relative difference in wind speed across the Pacific and is proportional to the reconstructed atmospheric pressure gradients.

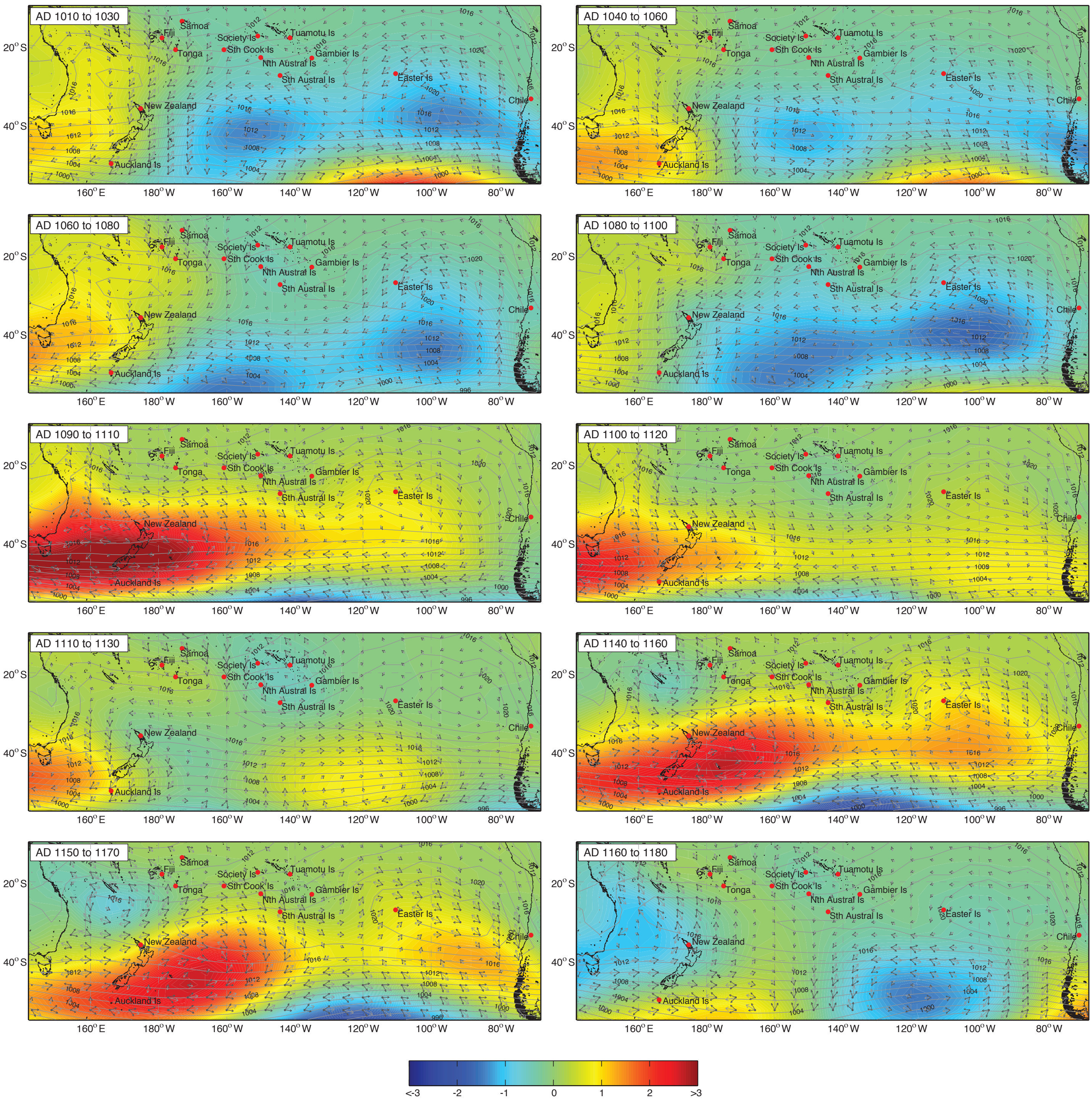

Figure S5b: Bi-decadal time period reconstructions. As for SI Appendix, Fig. S5a, but for selected periods between AD 1010 and 1180.

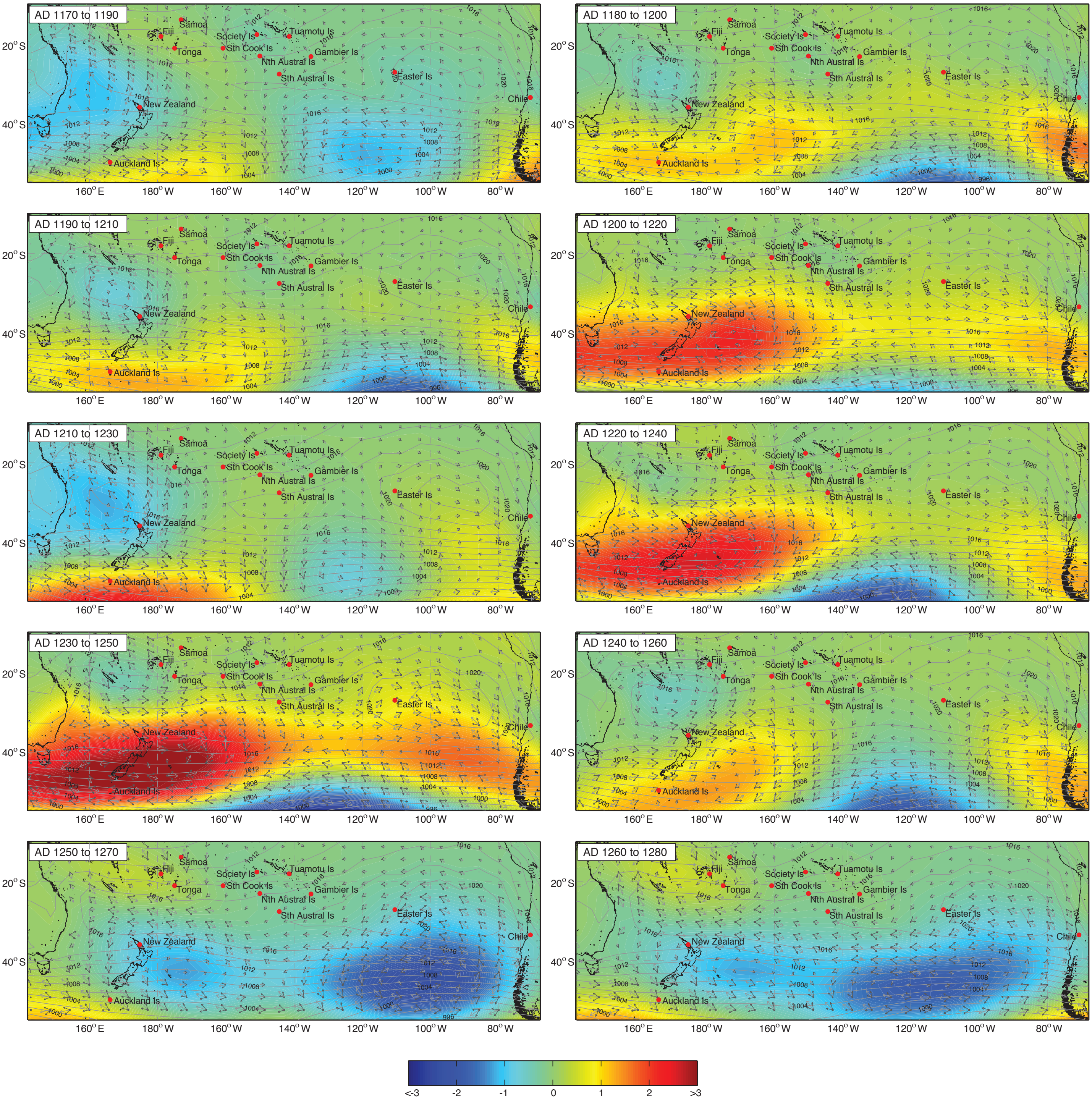

Figure S5c: Bi-decadal time period reconstructions. As for SI Appendix, Fig. S5a, but for selected periods between AD 1170 and 1280.

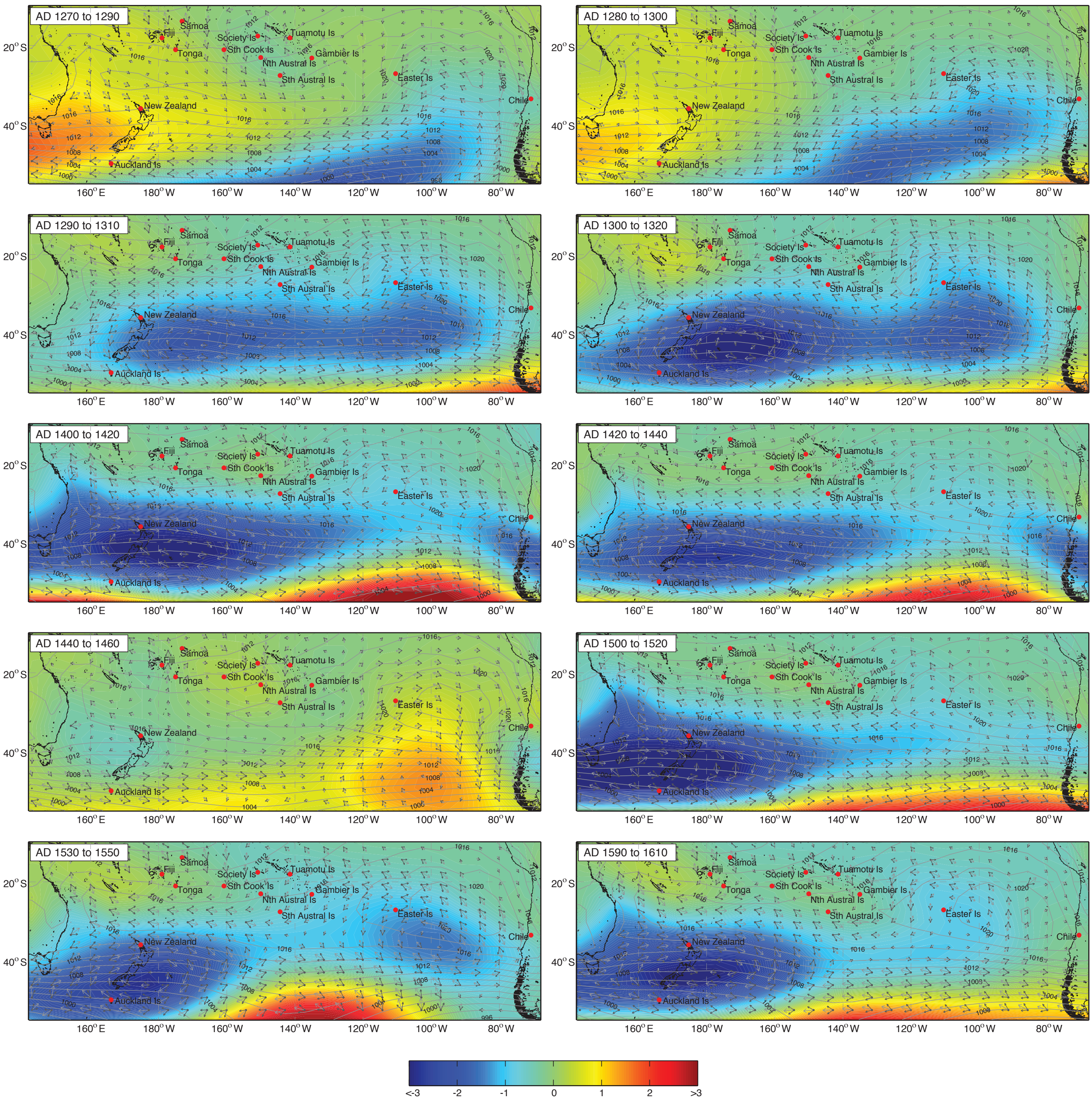

Figure S5d: Bi-decadal time period reconstructions. As for SI Appendix, Fig. S5a, but for selected periods between AD 1270 and 1610.

Supporting Table

Table S1: List of all proxy records included in the paleoclimate reconstruction.

Number	Location	Proxy	Proxy type	Climate Variable	Latitude (°)	Longitude (°)	Region	Reference
1	Lake Verlorenvlei	Sediment	Microfossil Diatom	Precipitation	-32	19	South Africa	1
2	Makapansgat Valley	Speleothem	$\delta^{18}O$	Precipitation	-24	28	South Africa	2
3	Flores, Indonesia	Speleothem	$\delta^{18}O$	Precipitation	-8	120	Indian Ocean	3
4	Rarotonga, Cook Islands	Coral	Density growth band	Sea Surface Temperature	-21	200	South Pacific	4
5	Vanuatu	Speleothem	$\delta^{18}O$	Precipitation	-18	168	South Pacific	5
6	Great Barrier Reef	Coral	$\delta^{18}O$	Precipitation	-18	146	Australia	6
7	Great Barrier Reef	Coral	Sr/Ca	Sea Surface Temperature	-18	146	Australia	6
8	Lake Frome, South Aust.	Sediment	Paleo lake volume	Precipitation	-30	139	Australia	7,8
9	Lake Surprise, Victoria	Sediment	Microfossil Diatom	Precipitation	-38	141	Australia	9
10	Coastal New South Wales	Sediment	Strandplain dune geometry	Wave Direction	-33	151	Australia	10
11	Mt Read Tasmania	Tree	Ring width	Temperature	-42	145	Australia	11
12	New Zealand Regional	Multiproxy	Multiple	Precipitation	-44	168	New Zealand	12
13	NZ South Island	Sediment	Glacial Moraine limit	Precipitation	-43.5	170	New Zealand	13
14	Oroko Swamp, South Island	Tree	Ring width	Temperature	-43	170	New Zealand	14
15	NZ North Island	Tree	Ring Width	Sea Level Pressure	-37	175	New Zealand	15
16	Urewera North Is.	Tree	Ring width	Temperature	-38	177	New Zealand	16
17	South America Regional	Multiproxy	Multiple	Precipitation	-40	287	South America	17
18	South America Regional	Multiproxy	Multiple	Temperature	-40	287	South America	18
19	Lago Guanaco, Chile,	Sediment	Carbonate	Precipitation	-52	287	South America	19

Table S1 (Continued)

Number	Location	Proxy	Proxy type	Climate Variable	Latitude (°)	Longitude (°)	Region	Reference
20	Laguna Aculeo, Chile	Sediment	Pigments	Temperature	-34	288	South America	20
21	South Orkney Is	Sediment	$\delta^{18}O$	Temperature	-60	314	South Atlantic	21
22	South Georgia Is	Sediment	Glacial Moraine limit	Temperature	-54	324	South Atlantic	22
23	Patagonia Chile and Argentina	Tree	Ring width	Precipitation	-41	289	South America	23
24	Droning Maude Land	Ice Core	$\delta^{18}O$	Temperature	-75	0.5	East Antarctica	24
25	Law Dome, Wilkes Land	Ice Core	Sodium (Na)	Sea Level Pressure	-66	112	East Antarctica	25
26	Law Dome, Wilkes Land	Ice Core	$\delta^{18}O$	Sea Level Pressure	-66	112	East Antarctica	26
27	Victoria Lower Glacier, Northern Victoria Land	Ice Core	δD	Temperature	-77	166	East Antarctica	27
28	Victoria Lower Glacier, Northern Victoria Land	Ice Core	Iron (Fe)	Sea Level Pressure	-77	166	East Antarctica	27
29	Victoria Lower Glacier, Northern Victoria Land	Ice Core	Sodium (Na)	Sea Level Pressure	-77	166	East Antarctica	27
30	Siple Dome	Ice Core	Sodium (Na)	Sea Level Pressure	-81	212	West Antarctica	28

References for SI Appendix

1. Stager JC et al. (2012) Precipitation variability in the winter rainfall zone of South Africa during the last 1400 yr linked to the austral westerlies. *Clim Past* 8:877–887.
2. Holmgren K et al. (1999) A 3000-year high-resolution stalagmite-based record of palaeoclimate for northeastern South Africa. *The Holocene* 9:295–309.
3. Griffiths ML et al. (2009) Increasing Australian–Indonesian monsoon rainfall linked to early Holocene sea-level rise. *Nature Geoscience* 2:636–639.
4. Goodwin ID, Harvey N (2008) Subtropical sea-level history from coral microatolls in the Southern Cook Islands, since 300 AD. *Marine Geology* 253:14–25.
5. Partin JW et al. (2013) Multidecadal rainfall variability in South Pacific Convergence Zone as revealed by stalagmite geochemistry. *Geology* 41:1143–1146.
6. Hendy EJ et al. (2002) Abrupt decrease in tropical Pacific sea surface salinity at end of Little Ice Age. *Science* 295:1511–1514.
7. Cohen TJ, Gliganic L, Lasren J, Goodwin ID, Browning S (2012) A pluvial episode identified in arid Australia during the Medieval Climatic Anomaly. *Quaternary Science Reviews*.
8. Cohen TJ et al. (2011) Continental aridification and the vanishing of Australia's megalakes. *Geology* 39:167–170.
9. Barr C (2010) Droughts and Flooding Rains: A fine-resolution reconstruction of climatic variability in western Victoria, Australia, over the last 1500 years. Dissertation (PhD thesis, University of Adelaide, Adelaide).
10. Goodwin ID, Stables MA, Olley JM (2006) Wave climate, sand budget and shoreline alignment evolution of the Iluka–Woody Bay sand barrier, northern New South Wales, Australia, since 3000 yr BP. *Marine Geology* 226:127–144.
11. Cook ER, Buckley BM, Palmer JG, Boswijk G (2006) Millennia-long tree-ring records from Tasmania and New Zealand: a basis for modelling climate variability and forcing, past, present and future. *J Quaternary Sci* 21:689–699.
12. Lorrey A, Salinger J, Palmer J, Neil H (2008) Speleothem stable isotope records interpreted within a multi-proxy framework and implications for New Zealand palaeoclimate reconstruction. *Quaternary International* 187:52–75.
13. Schaefer JM et al. (2009) High-frequency Holocene glacier fluctuations in New Zealand differ from the northern signature. *Science* 324:622–625.
14. Cook ER, Palmer JG, D'Arrigo RD (2002) Evidence for a "Medieval Warm Period"in a 1,100 year tree-ring reconstruction of past austral summer temperatures in New Zealand. *Geophys Res Lett* 29:1667.
15. Fowler A, Boswijk G, Gergis J, Lorrey A (2008) ENSO history recorded in Agathis australis (kauri) tree rings. Part A: kauri's potential as an ENSO proxy. *Int J Climatol* 28:1–20.
16. Xiong L, Palmer JG (2000) Reconstruction of New Zealand temperatures back to AD 1720 using Libocedrus bidwillii tree-rings. *Climatic Change* 45:339–359.
17. Neukom R et al. (2010) Multi-centennial summer and winter precipitation variability in southern South America. *Geophys Res Lett* 37:L14708.
18. Neukom R et al. (2010) Multiproxy summer and winter surface air temperature field reconstructions for southern South America covering the past centuries. *Climate Dynamics* 37:35–51.
19. Moy CM et al. (2008) Isotopic evidence for hydrologic change related to the westerlies in

SW Patagonia, Chile, during the last millennium. *Quaternary Science Reviews* 27:1335–1349.

20. Gunten von L, Grosjean M, Rein B, Urrutia R, Appleby P (2009) A quantitative high-resolution summer temperature reconstruction based on sedimentary pigments from Laguna Aculeo, central Chile, back to AD 850. *The Holocene* 19:873–881.
21. Noon PE, Leng MJ, Jones VJ (2003) Oxygen-isotope (δ18O) evidence of Holocene hydrological changes at Signy Island, maritime Antarctica. *The Holocene* 13:251–263.
22. Rosqvist GC, Schuber P (2003) Millennial-scale climate changes on South Georgia, Southern Ocean. *Quaternary Research* 59:470–475.
23. Villalba R (1990) Climatic fluctuations in northern Patagonia during the last 1000 years as inferred from tree-ring records. *Quaternary Research* 34:346–360.
24. Oerter H, Kipfstuhl S, Wilhelms F (2011) Stable isotope records for the past 1000 years from five ice cores in Central Dronning Maud Land. *IUGG*.
25. Goodwin ID, Van Ommen TD, Curran M, Mayewski PA (2004) Mid latitude winter climate variability in the South Indian and southwest Pacific regions since 1300 AD. *Climate Dynamics* 22:783–794.
26. Ommen TD, Morgan V (1996) Peroxide concentrations in the Dome summit south ice core, Law Dome, Antarctica. *Journal of Geophysical Research: Atmospheres (1984–2012)* 101:15147–15152.
27. Bertler NAN, Mayewski PA, Carter L (2011) Cold conditions in Antarctica during the Little Ice Age — Implications for abrupt climate change mechanisms. *Earth and Planetary Science Letters* 308:41–51.
28. Kreutz KJ et al. (2000) Sea level pressure variability in the Amundsen Sea region inferred from a West Antarctic glaciochemical record. *Journal of Geophysical Research: Atmospheres (1984–2012)* 105:4047–4059.